Research Article | Vol. 25, No. 21 | 16 Oct 2017 | OPTICS EXPRESS 25467
Optics EXPRESS

Very large photoresponsiviy and high photocurrent linearity for Ge-dot/SiO_2/SiGe photoMOSFETs under gate modulation

MING-HAO KUO,[1] PO-YU HONG,[2] PING-CHE LIU,[2] MENG-CHUN LEE,[2] HORNG-CHIH LIN,[2] TOM GEORGE,[1] AND PEI-WEN LI[1,2,*]

[1]*Department of Electrical Engineering, National Central University, ZhongLi, Taiwan*
[2]*Institute of Electrons Engineering and Department of Electronics Engineering, National Chiao Tung University, HsinChu, Taiwan*
**pwli@nctu.edu.tw*

Abstract: We report a novel visible–near infrared photoMOSFET containing a self-organized, gate-stacking heterostructure of SiO_2/Ge-dot/SiO_2/SiGe-channel on Si substrate that is simultaneously fabricated in a single oxidation step. Our typical photoMOSFETs exhibit very large photoresponsivity of 1000–3000A/W at low optical power (< 0.1μW) or large photocurrent gain of 10^3–10^8A/A with a wide dynamic power range of at least 6 orders of magnitude (nW–mW) linearity at 400–1250 nm illumination, depending on whether the photoMOSFET operates at V_G = + 3– + 4.5V or –1– + 1V. Numerical simulations reveal that photocarrier confinement within the Ge dots and the SiGe channel modifies the oxide field and the surface potential of SiGe, significantly increasing photocurrent and improving linearity.

OCIS codes: (160.4236) Nanomaterials; (220.4241) Nanostructure fabrication; (250.0040) Detectors; (250.5590) Quantum-well, -wire and -dot devices.

References and links

1. S. Wirths, R. Geiger, N. von den Driesch, G. Mussler, T. Stoica, S. Mantl, Z. Ikonic, M. Luysberg, S. Chiussi, J. M. Hartmann, H. Sigg, J. Faist, D. Buca, and D. Grützmacher, "Lasing in direct-bandgap GeSn alloy grown on Si," Nat. Photonics **9**(2), 88–92 (2015).
2. S. A. Srinivasan, M. Pantouvaki, S. Gupta, H. T. Chen, P. Verheyen, G. Lepage, G.r Roelkens, K. Saraswat, D. V. Thourhout, P. Absil, and J. V. Campenhout, "56 Gb/s germanium waveguide electro-absorption modulator," J. Lightwave Technol. **34**(2), 419–424 (2016).
3. A. Rickman, "The commercialization of silicon photonics," Nat. Photonics **8**(8), 579–582 (2014).
4. G. Chen, Y. Yu, X. Xiao, and X. Zhang, "High speed and high power polarization insensitive germanium photodetector with lumped structure," Opt. Express **24**(9), 10030–10039 (2016).
5. D. A. B. Miller, "Device requirements for optical interconnects to silicon chips," Proc. IEEE **97**(7), 1166–1185 (2009).
6. V. Sorianello, G. De Angelis, A. De Iacovo, L. Colace, S. Faralli, and M. Romagnoli, "High responsivity SiGe heterojunction phototransistor on silicon photonics platform," Opt. Express **23**(22), 28163–28169 (2015).
7. R. Going, T. J. Seok, J. Loo, K. Hsu, and M. C. Wu, "Germanium wrap-around photodetectors on Silicon photonics," Opt. Express **23**(9), 11975–11984 (2015).
8. A. M. Pravilov, *Radiometry in Modern Scientific Experiments* (Springer, 2011).
9. W. T. Lai, K. C. Yang, P. H. Liao, T. George, and P. W. Li, "Gate-stack engineering for self-organized Ge-dot/SiO_2/SiGe-shell MOS capacitors," Front. Mater. **3**, 1–9 (2016).
10. W. T. Lai, K. C. Yang, T. C. Hsu, P. H. Liao, T. George, and P. W. Li, "A unique approach to generate self-aligned SiO_2/Ge/SiO_2/SiGe gate-stacking heterostructures in a single fabrication step," Nanoscale Res. Lett. **10**(1), 224 (2015).
11. M. H. Kuo, M. C. Lee, H. C. Lin, T. George, and P. W. Li, "High photoresponsivity Ge-dot photoMOSFETs for low-power monolithically-integrated Si optical interconnects," Sci. Rep. **7**, 44402 (2017).
12. M. H. Kuo, W. T. Lai, T. M. Hsu, Y. C. Chen, C. W. Chang, W. H. Chang, and P. W. Li, "Designer germanium quantum dot phototransistor for near infrared optical detection and amplification," Nanotechnology **26**(5), 055203 (2015).
13. T. George, P. W. Li, K. H. Chen, K. P. Peng, and W. T. Lai, ""Symbiotic" semiconductors: unusual and counter-intuitive Ge/Si/O interactions," J. Phys. D Appl. Phys. **50**(10), 105101 (2017).

#306203 https://doi.org/10.1364/OE.25.025467
Journal © 2017 Received 1 Sep 2017; revised 3 Oct 2017; accepted 3 Oct 2017; published 5 Oct 2017

Optics EXPRESS

14. F. Prins, M. Buscema, J. S. Seldenthuis, S. Etaki, G. Buchs, M. Barkelid, V. Zwiller, Y. Gao, A. J. Houtepen, L. D. A. Siebbeles, and H. S. J. van der Zant, "Fast and efficient photodetection in nanoscale quantum-dot junctions," Nano Lett. **12**(11), 5740–5743 (2012).
15. S. Siontas, P. Liu, A. Zaslavsky, and D. Pacifici, "Noise performance of high-efficiency germanium quantum dot photodetectors," Appl. Phys. Lett. **109**(5), 053508 (2016).
16. J. Wang, M. Yu, G. Lo, D. L. Kwong, and S. Lee, "Silicon waveguided integrated germanium JFET photodetector with improved speed performance," IEEE Photonics Technol. Lett. **23**(12), 765–767 (2011).
17. R. W. Going, J. Loo, T. J. King, and M. C. Wu, "Germanium gate photoMOSFET integrated to silicon photonics," IEEE J. Sel. Top. Quantum Electron. **20**(4), 8201607 (2014).

1. Introduction

Recent progress in Si photonics technology including Ge/GeSn lasers [1], Si/Ge modulators [2], Ge/SOI waveguides [3], and Ge photodetectors [4], has offered promising solutions for the construction of monolithically-integrated Si optical interconnect systems for low-power and low-latency data transmission. One of key devices for the implementation of such systems is a compact-sized photodetector with high-photoresponsivity, broad bandwidth, and ultra-low capacitance [5], all of which properties are not yet readily achievable from either conventional Si or Ge photodiodes. A photodetector generally resides at the output terminal of a photonic system. The photodetector converts impinging light to electrical signals that are then fed into receiver circuits for further signal processing. In general, photodetectors are fabricated based on PN, PIN or avalanche diode structures because of the structural simplicity of these devices as well as the ease of fabrication. However, such photodiodes suffer from having high dark currents, occupying large areas, and/or operating at high voltages, thereby leading to substantial performance penalties such as higher power dissipation, device area, latency, and noise.

Apart from being a two-terminal photodiode, a phototransistor (PT) is a promising photodetector candidate because it provides high responsivity within small device areas thanks to its internal amplification [6, 7]. While PTs possess high responsivity for light, in general, they are not able to detect low levels of light any better than photodiodes [8]. That is, high photoresponsivity for a PT is gained at the expense of limited dynamic range of linearity.

In this paper, we report high photoresponsivity for low-power-level photodetection for visible to near infrared (NIR) illumination. Also, large photocurrent gain in combination with a wide dynamic range of linearity were experimentally demonstrated for our Ge-dot/SiO_2/SiGe photoMOSFET, depending on whether the photoMOSFET operates in the ON- or OFF-states under gate modulation. Numerical analysis of photocarrier density and energy band diagrams was conducted for understanding the high photoresponsivity and large photocurrent linearity for our photoMOSFETs under gate modulation.

2. Experiments

Our previous reports [9, 10] have experimentally demonstrated the formation of a self-organized, gate-stacking MOS heterostructure of SiO_2/Ge-dot/SiO_2/SiGe-shell using a CMOS-compatible nanofabrication approach. The key novelty of this gate-stacking heterostructure is that it is nanofabricated within a single oxidation step of SiGe nano-pillars that are lithographically patterned over a buffer Si_3N_4 layer on top of the Si substrate. Therefore, our approach effectively eliminates multiple, complicated microfabrication processes such as surface passivation and post-annealing, which are essential for the creation of conventional Ge MOS devices, prior to and following the deposition of gate-dielectric layers over the Ge. More importantly, our MOS gate-stack possesses good "tunability" for controlling the Ge-dot size, the interfacial SiO_2 thickness, and as well as the SiGe-shell composition and thickness. Thus, our one-step nanofabrication process provides a core building block for the practical fabrication of Ge-based MOS nanoelectronic [9, 10] and nanophotonic devices [11, 12]. The mechanisms for the formation of the Ge-dot/SiO_2/SiGe-shell gate-stacking structure as well as the process steps for the nanofabrication of our photoMOSFETs have been elaborated elsewhere [11, 12]. In this paper, we studied Ge-dot/SiO_2/SiGe-shell MOSFET

Optics EXPRESS

structures consisting of a 150nm-thick ITO transparent gate, a 35nm-thick control oxide layer of SiO_2, 90nm-diameter spherical Ge-dots, a 3.5 nm-thick interfacial layer of SiO_2 surrounding the Ge dots, and a 20nm-thick $Si_{1-x}Ge_x$ shell (x = 0.35–0.5) on the surface of a p-Si substrate, as shown in Figs. 1(a) and 1(b). The thickness of 3–4nm for the interfacial SiO_2 layer separating the Ge dot and the $Si_{1-x}Ge_x$ shell is a consequence of an exquisitely-controlled dynamic balance between the fluxes of oxygen and silicon interstitials [9-10, 13]. This interfacial oxide has high-quality structural integrity as confirmed by extensive transmission electron microscopy (TEM) and energy dispersive x-ray (EDX) examinations [9-10, 13]. Low interface trap densities (D_{it}) of 3–5 × 10^{11} cm^{-2}·eV^{-1} have been measured for the $SiO_2/Si_{1-x}Ge_x$ interface using frequency-dependent capacitance-voltage (C-V) characterization at various measurement temperatures [9]. The $Si_{1-x}Ge_x$ shell is created by the diffusion of Ge atoms from the Ge dot into the Si substrate and thus, is conformal with the spherical Ge dot and separated from it by the 3–4nm thick interfacial SiO_2 layer. Good crystallinity of the SiGe channel is evidenced by defect-free lattice fringes observed from HRTEM examinations [9] and from the selected area diffraction (SAD) patterns as shown in Fig. 1(c). The gate-length and gate-width of the Ge-dots MOSFETs are 3 μm and 70 μm, respectively.

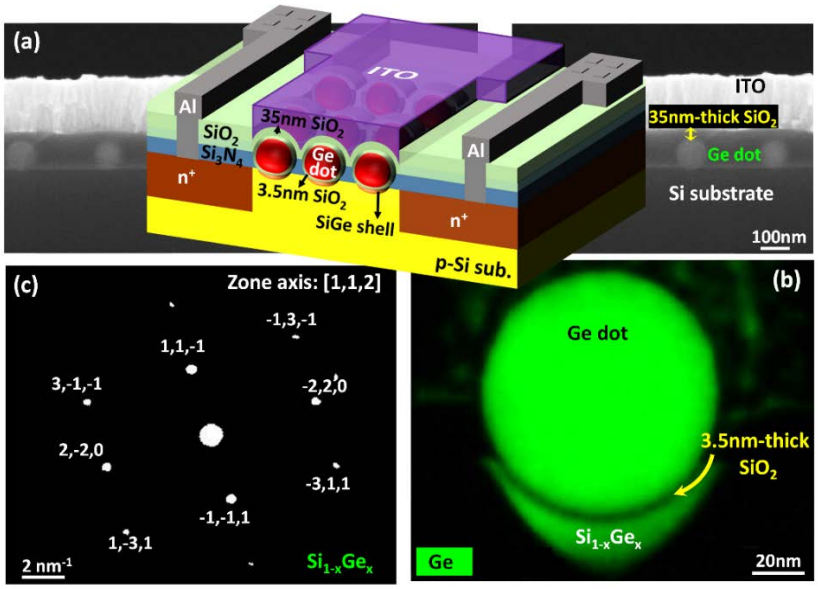

Fig. 1. Our Ge-dot MOSFETs are composed of a self-organized, gate-stacking heterostructure of a SiO_2/Ge-dot/SiO_2/SiGe-channel. (a) 3D schematic diagram and cross-sectional scanning electron microscopic micrograph of MOSFET structures with 90nm-Ge dots that (b) are separated from a 20nm-thick $Si_{1-x}Ge_x$ shell on the surface of a p-Si substrate by a 3.5nm-thick interfacial SiO_2 layer as evidenced by EDX elemental x-ray mapping micrograph highlighting the presence of Ge, and (c) SAD pattern analysis confirms good crystallinity of the $Si_{1-x}Ge_x$ shell.

3. Results

Figure 2(a) contains plots of the I_D-V_G characteristics of 90nm-diameter Ge-dot n-MOSFETs biased at V_D = + 2V and measured either in the dark or under 850nm variable-incident power (P_{IN}) illumination. In the dark, Ge-dot n-MOSFETs exhibit typical transfer curves with ON-OFF current ratio ($I_{dark,\ ON}$/ $I_{dark,\ OFF}$) as high as 2 × 10^7 for V_G ranging from –1V– + 5V. Here I_{OFF} and I_{ON} are drain currents measured at V_G = –1V (the so-called OFF-state, in which a negative gate bias makes the SiGe channel accumulate majority carriers (holes) between the $\boldsymbol{n}^+$–source and $\boldsymbol{n}^+$–drain) and at V_G = + 5V (the so-called ON-state, in which positive gate bias induces a conducting channel via charge inversion in the SiGe channel from holes to electrons), respectively. It is clearly seen that 850nm illumination at P_{IN} > 1μW does indeed increase drain

Optics EXPRESS

current across the entire experimental V_G range. Thanks to the extremely low dark current of 4 × 10^{-11}A in the OFF-state (V_G < + 1V), constant, V_G-independent photocurrent gain ($\boldsymbol{G}_{OFF}$ = $I_{OFF,\,photo}/I_{OFF,\,dark}$) values of as high as 10^3–10^8A/A were measured at P_{IN} = 6nW–250μW, as shown in Fig. 2(b). In contrast, $\boldsymbol{G}_{ON}$ ($I_{ON,\,photo}/I_{ON,\,dark}$) appears to be relatively smaller and have a strong dependence on V_G under similar variable-power illumination conditions.

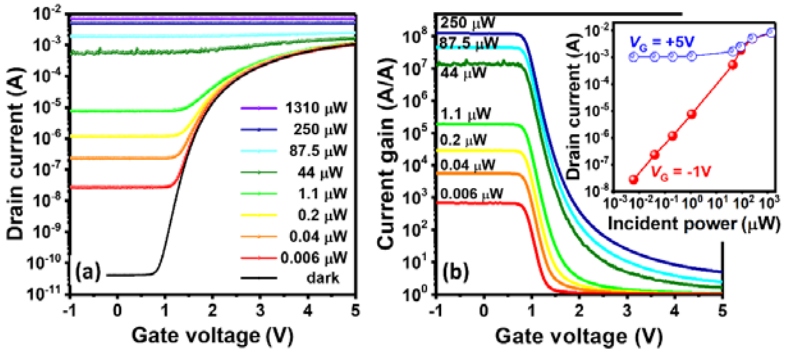

Fig. 2. (a) Experimentally-measured I_D-V_G characteristics of 90nm Ge-dot *n*-MOSFETs under variable-power 850nm illumination. (b) Large current gain was achieved for our Ge-dot MOSFETs when operating in both ON- and OFF-states. Inset shows that a wide dynamic range of photocurrent linearity of at least 6 decades is achievable for our Ge-dot MOSFET operating in the OFF-state, whereas a more limited range of linearity is measured for operation in the ON-state.

For 600–1250 nm illumination, photoresponsivities ($\mathfrak{R} \equiv (I_{photo}–I_{dark})/P_{IN}$) for the Ge-dot photoMOSFETs appear to have a nearly constant $\mathfrak{R}_{OFF}$ over the experimental V_G range of –1V– + 1V (*i.e.*, in the OFF-state). Figure 3(a) shows that $\mathfrak{R}_{ON}$ increases sharply at V_G = + 1V (*i.e.*, when the conducting channel is electrically turned on), and reaches a maximal value ($\mathfrak{R}_{ON,\,max}$) at approximately V_G = 3V–4.5V. $\mathfrak{R}_{ON,\,max}$ appears to have a strong dependence on the value of the incident optical power, P_{IN}. For instance, for 850nm illumination, $\mathfrak{R}_{ON,\,max}$ decreases with an increase in P_{IN} ranging from 6nW–87.5μW, and then asymptotically approaches a saturation value of approximate 20A/W at $P_{IN} \geq$ 87.5μW as shown in Fig. 3(b). While a very large value of $\mathfrak{R}_{ON,\,max}$ = 1,400A/W is achievable for low-level illumination (P_{IN} < 10nW) by Ge-dot PTs operating in the ON-state, $\mathfrak{R}_{OFF}$ appears to have a mild increase from 6–20 A/W for P_{IN} ranging from 6nW–1.4mW. Both Figs. 2 and 3 suggest that a wide dynamic range of photocurrent linearity of at least 6 decades is achievable for our Ge-dot MOSFET operating in the OFF-state, whereas a more limited range of linearity is measured for operation in the ON-state.

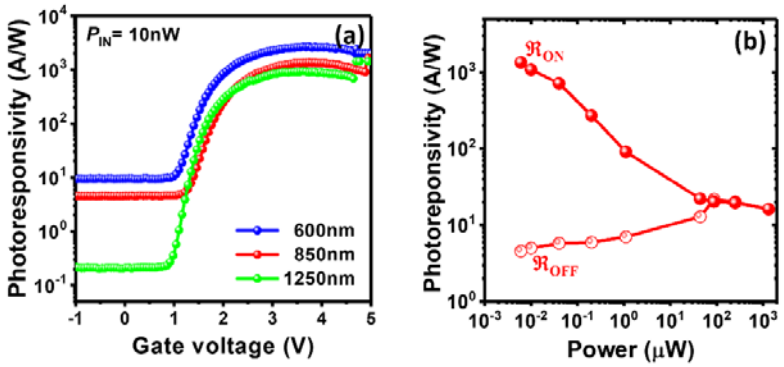

Fig. 3. (a) Photoresponsivity $\mathfrak{R}$-V_G characteristics of 90nm Ge-dot *n*-PTs under P_{IN} = 10nW, 600-1250nm illumination, and (b) Power-dependent photoresponsivity for the Ge-dot MOSFET operating in the ON-state and OFF-states for 850nm illumination.

Optics EXPRESS

Figure 4(a) shows that for low-level illumination at P_{IN} = 10nW, broad spectral photoresponse from near ultraviolet (NUV) to near infrared (NIR) is measured on our Ge-dot photoMOSFETs. Very high photoresponsivity values of $\mathfrak{R}_{ON}$ = 1000–3000A/W and reasonably large $\mathfrak{R}_{OFF}$ = 1–20A/W were measured at illumination wavelengths (λ) ranging from 400–1250nm. Both spectral responses, $\mathfrak{R}_{ON}$ and $\mathfrak{R}_{OFF}$, follow the spectral behavior for the absorption coefficient for bulk Ge. It is a known fact that the cut-off wavelength for the spectral response of a photodetector is determined by the intrinsic material properties of the absorption layer, in particular, the bandgap energy and absorption coefficient. The cut-off wavelength of 1250nm for our Ge-dot MOSFET is greater than that (< 1100nm) for a conventional Si MOSFET [8], indicating that the photoresponse of our devices is dominated by the photoresponse of the Ge dots and the SiGe shell rather than the Si substrate. Our experimental demonstration of very large photocurrent gain and photoresponsivity in our Ge-dot/SiO_2/SiGe MOSFETs suggests that Ge dots and SiGe shells enable superior photoelectric conversion. This is evidenced by high values of 100–400 and 10–50 for the modulated charges generated per incident photon in the visible and NIR regimes, respectively. These values are based on the calculation of $\mathfrak{R} \times (hc/e\lambda)$ [14], where h is Planck's constant, c is the speed of light, and e is the electron charge.

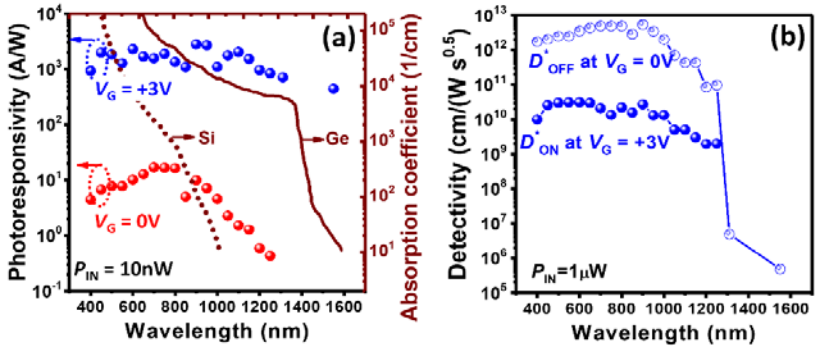

Fig. 4. Wavelength-dependent (a) photoresponsivity and (b) detectivity for 90nm Ge-dot *n*-MOSFETs operating in the OFF-state (V_G = 0V), and ON-state (V_G = + 3V) measured under 400–1550nm illumination. Both spectral behaviors follow the wavelength dependence of absorption coefficient of bulk Ge.

At medium-level operating of P_{IN} = 1μW, shot noise from the dark current is assumed to dominate all other sources of noise in our device [15]. We were able to estimate the specific detectivity (D^*) by the calculation of $D^* = \mathfrak{R}(A/2eI_{dark})^{0.5}$ [15], where A is the channel area. The calculated wavelength dependent D^*_{ON} and D^*_{OFF} spectra for our Ge–dot PTs operating in the ON-states and OFF-states, respectively, are displayed in Fig. 4(b). It is clearly seen that high values of $D^*_{OFF} = 10^{12}$–10^{13} cm/(W·s$^{1/2}$) and $D^*_{OFF} = 10^{11}$–10^{12} cm/(W·s$^{1/2}$) in the NUV–visible (400–1000nm) and NIR (1000–1200nm) regimes, respectively, were estimated for our Ge-dot photoMOSFET operating in the OFF-state. The D^*_{OFF} spectral response curve lies well above the D^*_{ON} curve by at least two orders of magnitude. This is because that while $\mathfrak{R}_{ON,max}$ is higher than $\mathfrak{R}_{OFF}$ by a factor of approximately 100–1000, dark current in the OFF-state is far less than that in the ON-state by 7 orders in magnitude (recall that the ON-OFF ratio, $I_{dark, ON}/I_{dark, OFF}$, is as high as 10^7).

4. Discussion

We carried out numerical analysis in order to determine the respective contributions of Ge dots and the SiGe channels on the gain and linearity of photocurrents measured for our Ge-dot/SiO_2/SiGe photoMOSFETs. This numerical analysis in terms of potential energy and carrier density was conducted for three different MOS structures, namely (a) ITO/SiO_2/Si, (b)

Optics EXPRESS

ITO/SiO_2/$Si_{0.5}Ge_{0.5}$-on-Si, and (c) ITO/SiO_2/Ge-dot/SiO_2/$Si_{0.5}Ge_{0.5}$-on-Si, both for operation in the dark and under illumination, respectively, using a Silvaco Atlas TCAD simulator. For conventional *n*-Si MOSFETs operating at V_G = + 3V (*i.e.*, in the ON-state) in the dark, the *E*-field generated by a positive V_G depletes the majority carrier (hole) at the surface of the Si substrate, and attracts minority carriers (electron) from the bulk to migrate to the surface. Consequently, the charge polarity of the Si surface is inverted from nominally *p*-type (hole) to *n*-type (electron), thereby forming an electron channel connecting the $\boldsymbol{n}^+$-source and $\boldsymbol{n}^+$-drain as shown in Fig. 5(a). Figure 5(b) shows that for the ITO/SiO_2/$Si_{0.5}Ge_{0.5}$-on-Si devices, the creation of a 20nm-thick $Si_{0.5}Ge_{0.5}$ layer at the surface of the Si substrate inherently generates a potential well for holes due to the large valence band offset (~0.3eV) at the SiGe/Si interface. Figure 5(c) shows that Ge dots embedded within the gate oxide layer also generate a deep potential well for confining both electrons and holes such that the *E*-field across the gate-stacking heterostructure and the surface potential energy of the SiGe well are both modified for the ITO/SiO_2/Ge-dot/SiO_2/SiGe/Si MOSFETs.

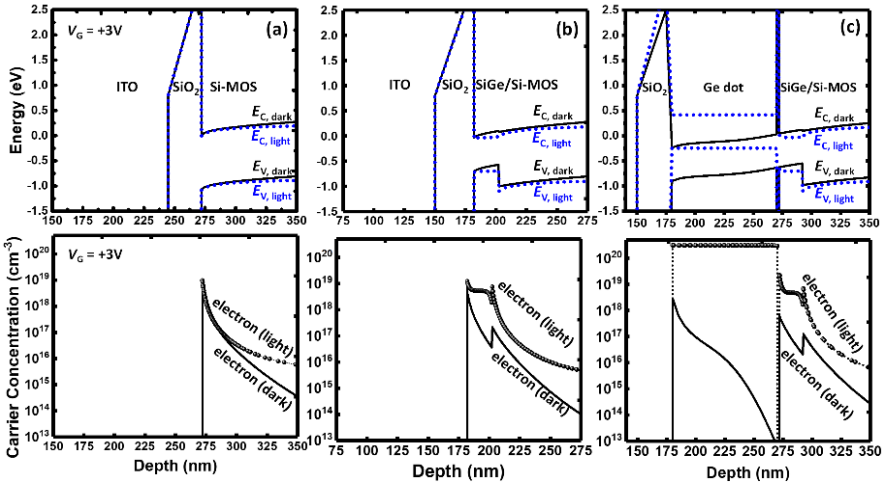

Fig. 5. Calculated energy band diagrams and carrier concentrations for three different MOS structures: (a) ITO/SiO_2/Si, (b) ITO/SiO_2/$Si_{0.5}Ge_{0.5}$-on-Si, and (c) ITO/SiO_2/Ge-dot/SiO_2/$Si_{0.5}Ge_{0.5}$-on-Si, all devices operating at V_G = + 3V both in the dark and under illumination, respectively. Solid and dashed lines denote potential energy and electron density for the MOSFETs operating in the dark and under 850nm illumination, respectively.

A low absorption coefficient at 850nm illumination for conventional *n*-Si MOSFETs results in the generation of very few photo-electrons and photo-holes at the surface of the Si substrate, as shown in Fig. 5(a). However, the same 850nm illumination induces a dramatic change in the surface potential and charge density for our MOSFETs containing both SiGe well and Ge dots due to their high absorption coefficients and the as-formed potential wells described above. This is because not only is the SiGe-shell able to efficiently absorb 850nm light and generate high concentrations of photo-electrons and photo-holes, but also more importantly, the confinement of photo-holes within the SiGe well induces a lowering in the surface potential energy, which in turn increases the surface electron density as shown in Fig. 5(b). Furthermore, the high absorption coefficient and its quasi-direct band gap structure make the Ge dots generate a significantly higher density of photocarriers that exceeds the photo-hole density within the SiGe by several orders of magnitude. The confinement of high-density photocarriers within the Ge dots significantly increases the potential energy of the Ge dot, which in turn, enhances the *E*-field within the interfacial oxide (between the Ge dot and the SiGe channel), lowers the SiGe surface potential, and increases the surface electron density for the SiGe well.

Figure 6(a) shows that an increase in optical power progressively generates excess photocarriers within the Ge dots and the SiGe well. It is important to note that in contrast to a

Optics EXPRESS

lowering in the potential energy for the SiGe well due solely to hole confinement, the storage of photocarriers within the Ge dot significantly increases the local potential energy of the Ge dots, modifying the *E*-fields within the gate oxide layers such that both the *E*-field across the interfacial oxide and the *E*-field across the control oxide near the gate electrode are increased. In combination with the oxide field modification, the surface potential energy for the SiGe well rises for $P_{IN} \geq 2.4\mu W$, counteracting the lowering in potential energy for the SiGe well induced by the excess photo-hole confinement. Thus, both an increase in the surface potential energy and a reduction in electron density near the surface of the SiGe well occurs for $P_{IN} \geq 21\mu W$, resulting in a limited dynamic range for photocurrent linearity for the Ge-dot MOSFETs operating in the ON-state.

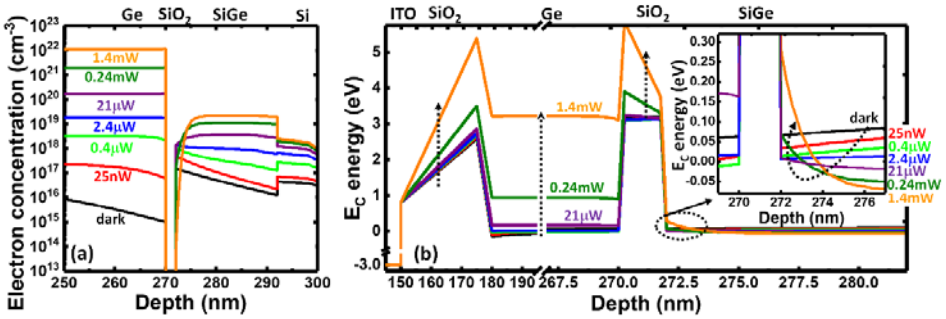

Fig. 6. Calculated (a) carrier concentrations and (b) conduction-band potential energies of ITO/SiO_2/Ge-dot/SiO_2/$Si_{0.5}Ge_{0.5}$-on-Si operating at V_G = + 3V in the dark and under variable power 850nm illumination. The inset in (b) is the enlarged diagram of conduction-band potential energy showing the surface potential energy near the SiO_2/SiGe channel being effectively varied as a function of the incident optical power under 850nm illumination.

The influence of the SiGe channel and Ge dot characteristics on the modification of the potential energy and carrier density becomes further enhanced for MOSFETs operating in the OFF-state. Figure 7(a) shows the energy band diagram and carrier distribution for a conventional Si *n*-MOSFET operating at $V_G = -2V$ in the dark. A negative gate bias induces an upward band bending at the surface of *p*-Si substrate, leading to majority carrier, *i.e.* hole accumulation at the surface of the Si and therefore no conducting channel between the $\boldsymbol{n}^+$-source and $\boldsymbol{n}^+$-drain. Figure 7(b) shows that for ITO/SiO_2/$Si_{0.5}Ge_{0.5}$-on-Si devices, hole confinement within the SiGe well induces a considerable lowering in the surface potential energy, which is in contrast to the previously-mentioned upward band bending near the surface for ITO/SiO_2/Si MOSFETs. Ge dots embedded within the gate oxide layers modify the oxide *E*-fields, leading to a further decrease of the surface potential energy and increase in the electron density within the SiGe shell for our devices, as shown in Fig. 7(c). Despite the fact that the inclusion of SiGe shells and Ge dots increases the surface electron density by 6 orders of magnitude (*i.e.*, from $10^3 cm^{-3}$ for Si MOSFETs shown in Fig. 7(a) to $10^9 cm^{-3}$ for the SiGe well shown in Figs. 7(b) and 7(c)) for operation in the dark, the surface electron density is still far less than the majority carrier (hole) density by several orders in magnitude for MOSFETs biased at $V_G = -2V$.

Optics EXPRESS

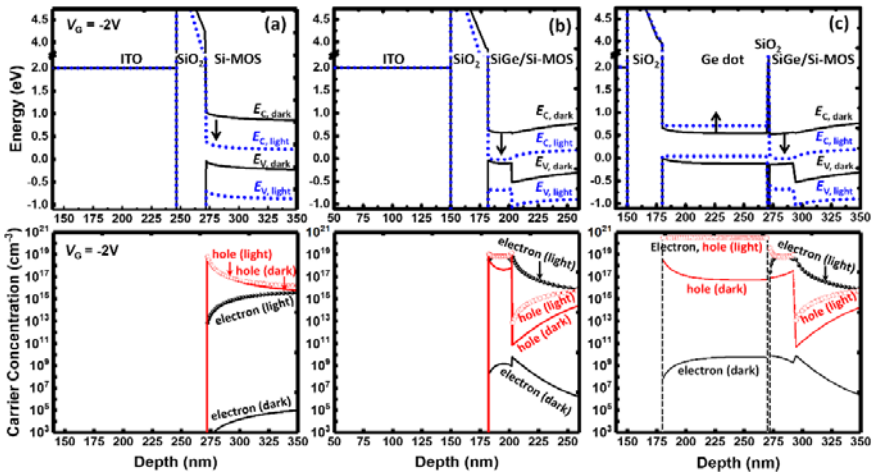

Fig. 7. Calculated energy band diagrams and carrier concentrations for three different MOSFETs of (a) ITO/SiO_2/Si, (b) ITO/SiO_2/$Si_{0.5}Ge_{0.5}$-on-Si, and (c) ITO/SiO_2/Ge-dot/SiO_2/$Si_{0.5}Ge_{0.5}$-on-Si operating at V_G = –2V in the dark and under illumination, respectively. Solid and dashed lines denote potential energy and electron density for the MOSFETs operating in the dark and under 850nm illumination, respectively.

Illumination does indeed provide another degree of freedom, or an effective optical-gate for modulating the oxide *E*-fields, surface potential, and most importantly, the surface charge polarity and density for Ge-dot photoMOSFETs that are electrically-biased in the OFF-state. Illumination essentially induces a considerably large lowering (~0.6eV) in surface potential energy for all our MOSFETs operating in the OFF-states in comparison to the ON-state (~0.1eV). Again, the low absorption coefficient for Si under 850nm illumination does not change the charge polarity near the surface of the Si substrate, as shown in Fig. 7(a), whereas Fig. 7(b) shows that the 850nm light excites a large number of photocarriers within the SiGe well. Thus, an electron channel connecting source and drain is "optically" created even though the ITO/SiO_2/$Si_{0.5}Ge_{0.5}$-on-Si MOSFET is electrically biased in the OFF-state. Ge dots further enable the effectiveness of the "optical gating" for the MOSFET. This is evidenced by a significant increase in the local potential energy of the Ge dot as shown in Fig. 7(c), as well as noticeable modifications of the oxide *E*-fields, the surface potential energy, and even the surface charge density of the SiGe well as shown in Fig. 8. Notably, the amplitude and polarity of the oxide *E*-field near the gate electrode appear to have a strong dependence on the optical power. That is, an increasing concentration of photocarriers within the Ge dots gives rise to a continuous increase in the local potential energy of the Ge dot, inducing an increasing built-in *E*-field across the control oxide layer, and which is in opposite direction to the externally-applied *E*-field. As a consequence, the net oxide *E*-field near the ITO gate electrode is reduced in amplitude by increasing the optical power and even undergoes a polarity change at $P_{IN} \geq 600$ μW, as shown in Fig. 8(b). On the contrary, the *E*-field across the interfacial oxide between the Ge dot and the SiGe well is monotonically increased with a progressive rise in the local potential of the Ge dot. This local potential rise is induced by increasing the incident optical power, which, in turn, modifies the surface potential energy of the SiGe well. Again, the Ge-dots-induced rise in surface potential of the SiGe well occurs and is offset by the large potential energy lowering (~0.7eV) due to photo-hole confinement within the SiGe well. These effects result in an ultimate reduction in the electron density at the surface of the SiGe well for $P_{IN} \geq 120$ μW.

Optics EXPRESS

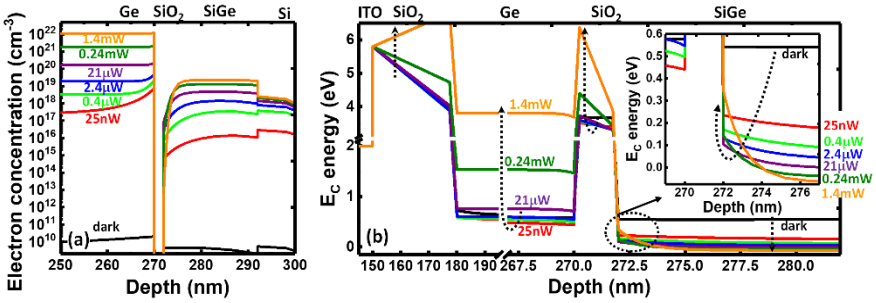

Fig. 8. Calculated (a) carrier concentration and (b) conduction-band potential energies for ITO/SiO_2/Ge-dot/SiO_2/$Si_{0.5}Ge_{0.5}$-on-Si MOSFETs operating at V_G = –2V in the dark and under illumination, respectively. The inset in (b) is the enlarged diagram of conduction-band potential energy showing the surface potential energy near the SiO_2/SiGe channel being effectively varied as a function of the incident optical power under 850nm illumination.

Numerical analysis reveals that for our Ge-dot/SiO_2/SiGe MOSFETs, optical power effectively modifies the surface potential and the surface charge density of the SiGe well. Figure 9 shows the simulated surface charge density per unit incident optical power ($(\boldsymbol{n}_{light}–\boldsymbol{n}_{dark})/P_{IN}$), which is proportional to photoresponsivity, for the Ge-dot MOSFETs operating at V_G = –2V and V_G = + 3V. It is noted that for incident $P_{IN} \leq 100$ μW, Ge-dot MOSFETs operating in the OFF-state have a nearly constant $(\boldsymbol{n}_{light}–\boldsymbol{n}_{dark})/P_{IN}$, whereas the photocarrier density per unit incident optical power decreases rapidly for increasing P_{IN} for the Ge-dot MOSFET operating in the ON-state. Therefore, our simulation results are in good agreement with our experimentally measured data shown in Fig. 3(b).

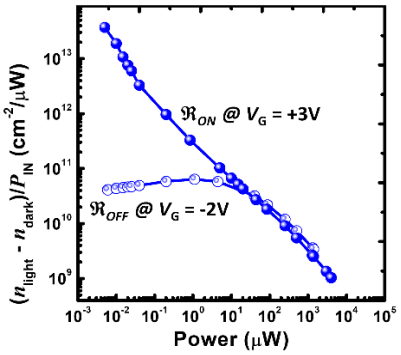

Fig. 9. Simulated surface charge density per unit excitation optical power plotted as a function of the incident illumination power. Note the decrease of this parameter with increasing illumination power, which is in good agreement with our experimentally-observed results.

5. Conclusions

In summary, our Ge-dot/SiO_2/SiGe phototransistors that are electrically biased in the ON-state ($V_G \approx$ + 3V) exhibit very large photoresponsivity of >1200 A/W and 441 A/W for low-light-level photodetection at 0.1μW for 850nm and 1550nm illumination, respectively. Our Ge-dot/SiO_2/SiGe MOSFETs have also demonstrated superior photocurrent linearity with a wide dynamic range of at least 6 orders in excitation power, high photoresponsivity that is nearly immune to fluctuations in either the bias voltage (V_G) or threshold voltage (V_{TH}), and low dark currents ($I_{OFF,\ dark}$) of less than 10^{-10}A while operating in the OFF-states. Table 1 summarizes the performance of previously reported Ge photodetectors based on Ge NPN transistor [7], Ge junction field-effect transistor (JFET) [16], Ge-gate MOSFET [17], and our own devices. Compared to other phototransistors, our Ge-dot MOSFET exhibits very large photoresponsivity and current gain at low-level operating power. This experimental

Optics EXPRESS

demonstration suggests that our Ge-dot phototransistors operating at low V_G (–1V– + 1V) can be considered as an effective, "building block" component for photodetection in practical receiver circuitry thanks to its low power consumption, high photoresponse stability, and high detectivity.

Table 1. Performance comparison of previously reported Ge phototransistors and our Ge-dot photoMOSFETs

Transistor	Operating power(W)	Responsivity (A/W) @1550nm	current gain (A/A)	Waveguided	Reference
Ge NPN transistor	5μW	14@1.5V	1.41	yes	[7]
Ge JFET	1mW	0.017@1V	84.8	yes	[16]
Ge-gate nMOSFET	0.583μW	18@1V	1.084	yes	[17]
	468μW	0.142@1V	1.46		
Ge-dot pMOSFET	7 nW	268@-4V	1.02	no	[11]
	0.33μW	20.1@-4V	1.07		
	8.4μW	1.09@-4V	1.096		
	425μW	0.03@-4V	1.133		
	1.06mW	0.015@-4V	1.163		
	7 nW	1.79E-05@0.5V	1.0006		
	0.33μW	1.94E-06@0.5V	1.0029		
	8.4μW	9.61E-07@0.5V	1.0369		
	425μW	8.06E-07@0.5V	2.5634		
	1.06mW	1.12E-06@0.5V	6.43		
Ge-dot nMOSFET	7 nW	441.3@3V	1.027	no	This work
	0.33μW	38.6@3V	1.078		
	8.4μW	1.78@3V	1.09		
	425μW	0.0375@3V	1.095		
	1.06mW	0.017@3V	1.105		
	7 nW	2.41E-05@-0.5V	1.0004		
	0.33μW	1.05E-06@-0.5V	1.004		
	8.4μW	4.25E-08@-0.5V	1.06		
	425μW	5.9E-08@-0.5V	4.1		
	1.06mW	1.1E-07@-0.5V	13.2		

Funding

Ministry of Science and Technology of Republic of China (MOST 105-2221-E-009-134-MY3 and 106-2633-E-009-001); Asian Office of Aero-space Research and Development (FA 2386-15-1-4025).